

## Supporting Information

# **Tumor Microenvironment-Triggered In-Situ Cancer Vaccines with Dual Immunogenic Cell Death Inductions for Elevated Antitumor and Antimetastatic Therapy**

Binbin Ding<sup>a</sup>, Pan Zheng<sup>a</sup>, Dong Li<sup>c</sup>, Meifang Wang<sup>a</sup>, Fan Jiang<sup>a,b</sup>, Zhanfeng Wang<sup>d</sup>, Ping'an Ma<sup>\*,a,b</sup>,  
Jun Lin<sup>\*,a,b</sup>

<sup>a</sup> *State Key Laboratory of Rare Earth Resource Utilization, Changchun Institute of Applied Chemistry, Chinese Academy of Sciences, Changchun, 130022, China*

<sup>b</sup> *University of Science and Technology of China, Hefei, 230026, China*

<sup>c</sup> *College of Basic Medical Sciences, Jilin University, Changchun, 130021, China*

<sup>d</sup> *Department of Neurosurgery, The Third Hospital of Jilin University, Changchun, 130033, China*

**Chemicals.** All chemical reagents were used directly without further purification. 1-hexanol (98%), n-dodecane and concentrated H<sub>2</sub>O<sub>2</sub> (30%) were purchased from Aladdin. Pentacarbonyl iron (Fe(CO)<sub>5</sub>, >97%) was purchased from Aldrich. Diethylene glycol and hexadecyltrimethylammonium bromide (CTAB) were purchased from Sinopharm chemical reagent co. LTD. Oxaliplatin (Oxp, >99%) was purchased from Meilunbio. DSPE-PEG<sub>2000</sub>-NH<sub>2</sub> was obtained from Ponsure Biotechnology (Shanghai).

**Cell lines and animals.** 4T1 cells were first cultured in Dulbecco's Modified Eagle's Medium (DMEM) supplemented with 10% heat-inactivated fetal bovine serum (FBS, GIBCO), 100 units per mL of penicillin and 100 units per mL of streptomycin (Sigma) in an atmosphere of 5% CO<sub>2</sub> at 37 °C. Female Balb/c mice (19-22 g) were purchased from the Center for Experimental Animals, Jilin University (Changchun, China). All mice were handled using the protocol approved by the Institutional Animal Care and Use Committee of Jilin University.

**Material Characterization.** The transmission electron microscopy (TEM) images of samples were obtained using a FEI Tecnai G2 S-Twin with a field emission gun operating at 200 kV. Their crystal structure was determined by X-ray powder diffraction (Bruker) equipped with Cu-K $\alpha$  radiation ( $\lambda=0.154$  nm). The X-ray photoelectron spectra (XPS) were taken on a VG ESCALAB MK II electron spectrometer using Mg K $\alpha$  (1200 eV) as the excitation source. Concentrations of Fe and Pt were tested by inductively coupled plasma-mass spectrometer (ICP-MS) or inductively coupled plasmaoptical emission spectrometer (ICP-OES). The dynamic light scattering was performed on a Malvern instrument Zetasizer Nano. The flow-cytometry assay was performed on a Flow Cytometer (guava easyCyte™).

**Statistical Analysis.** Analysis of variance (ANOVA) was used to assess statistical significance.

\*p<0.05, \*\*p< 0.01, \*\*\*p<0.001.

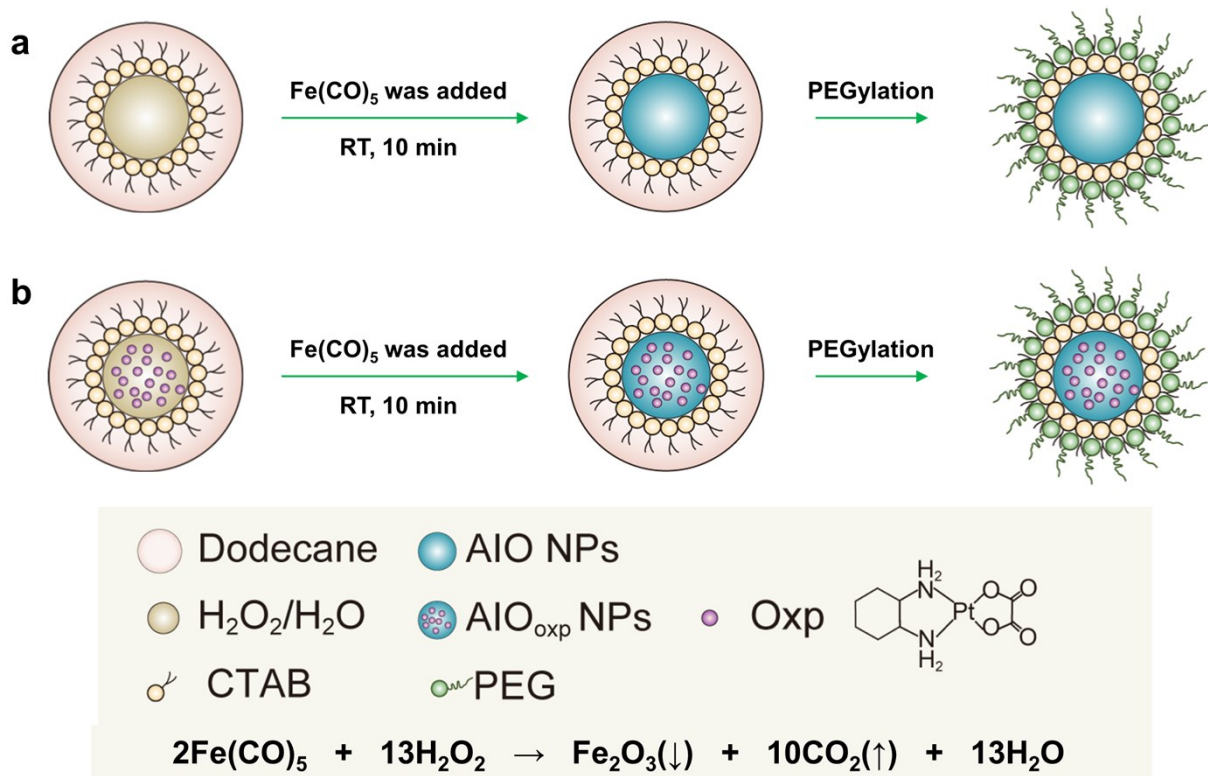


**Figure S1.** Schematic presentations of synthesis of (a) AIO NPs and (b) AIO<sub>oxp</sub> NPs by a reversed microemulsion (water-in-oil) method at room temperature (RT) using Fe(CO)<sub>5</sub> as a reducing agent and H<sub>2</sub>O<sub>2</sub> as an oxidizing agent.

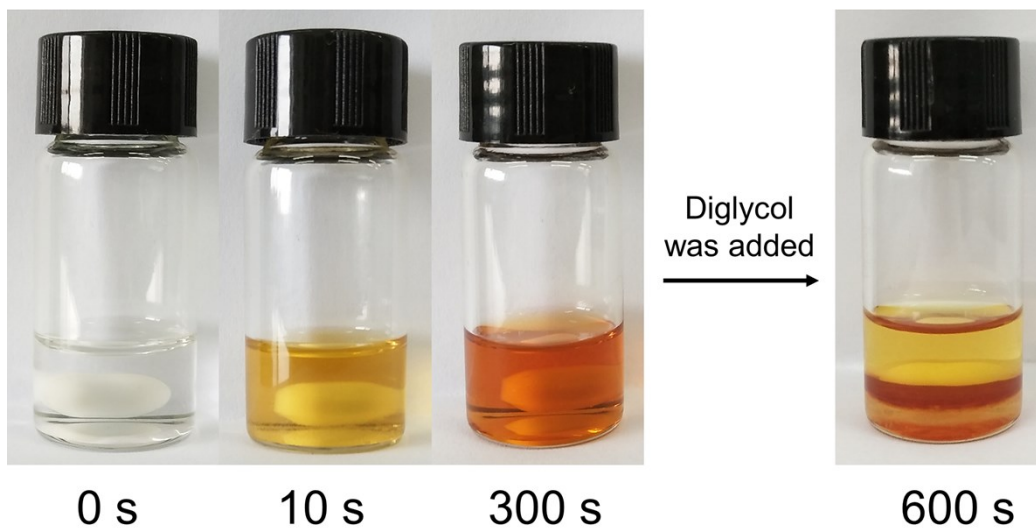


**Figure S2.** Digital photographs of reaction solution at different time point (0, 10, 300, 600 s). At 600 s, diglycol was added and the deep brown product could be seen.

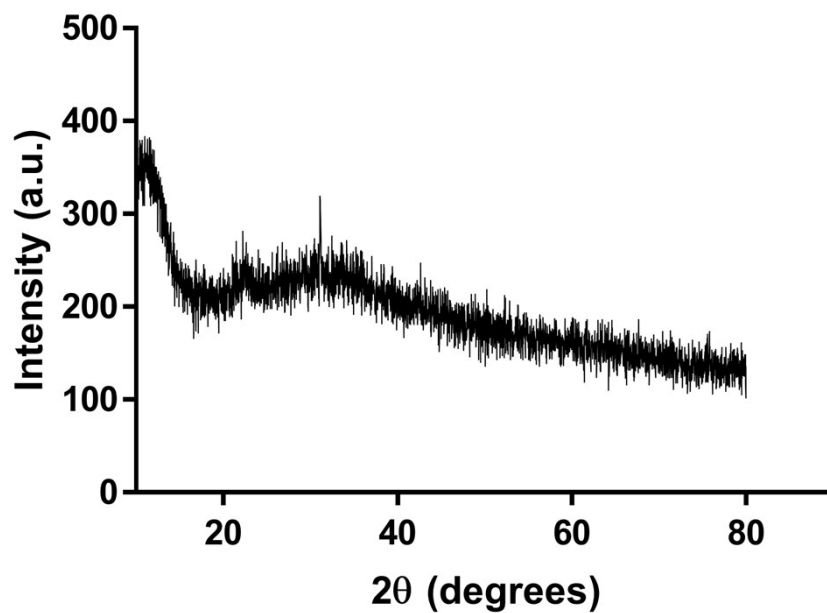


**Figure S3.** XRD pattern of AIO NPs.

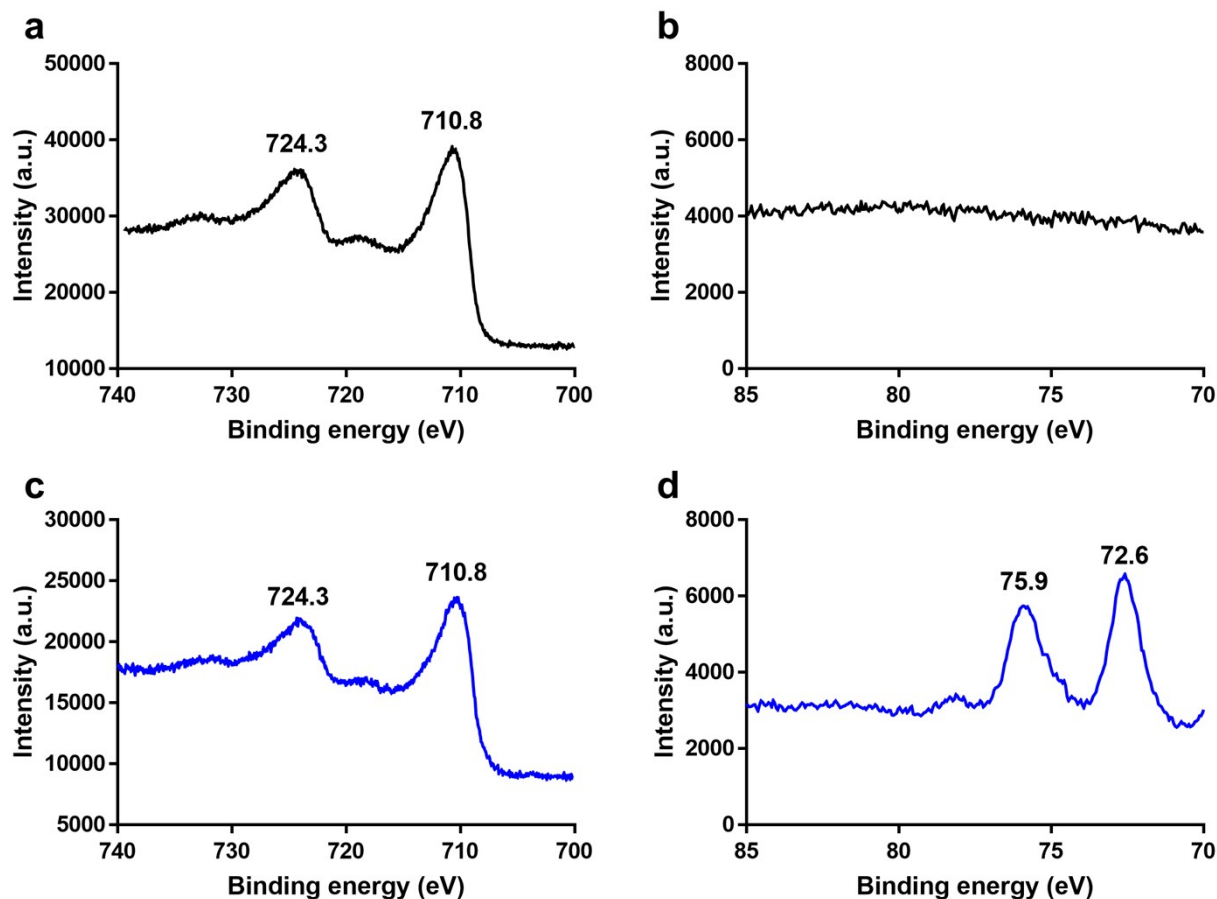


**Figure S4.** X-ray photoelectron spectroscopy (XPS) high-resolution scans of Fe 2p peaks in (a) AIO NPs and (c) AIO<sub>oxp</sub> NPs. The two characteristic peaks located at 724.3 eV (Fe 2p<sub>1/2</sub>) and 710.8 eV (Fe 2p<sub>3/2</sub>) are assigned to Fe<sup>3+</sup>, suggesting that the obtained products are Fe<sub>2</sub>O<sub>3</sub>. XPS high-resolution scans of Pt 4f peaks in (b) AIO NPs and (d) AIO<sub>oxp</sub> NPs. Compared with AIO NPs, the appearance of Pt 4f peaks in AIO<sub>oxp</sub> NPs suggests Oxp is successfully loaded into AIO NPs.

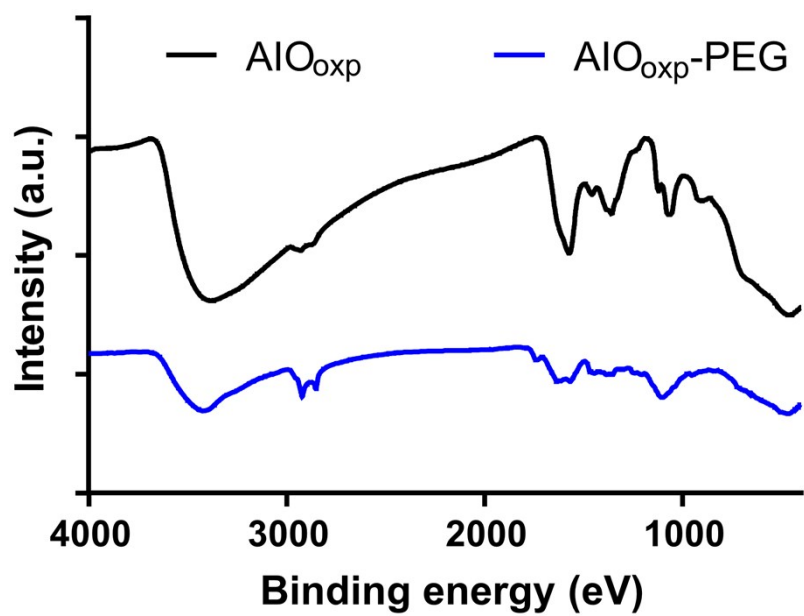


**Figure S5.** Fourier transform infrared spectroscopy (FTIR) of  $\text{AlO}_{\text{oxp}}$  NPs with or without PEG modifications.

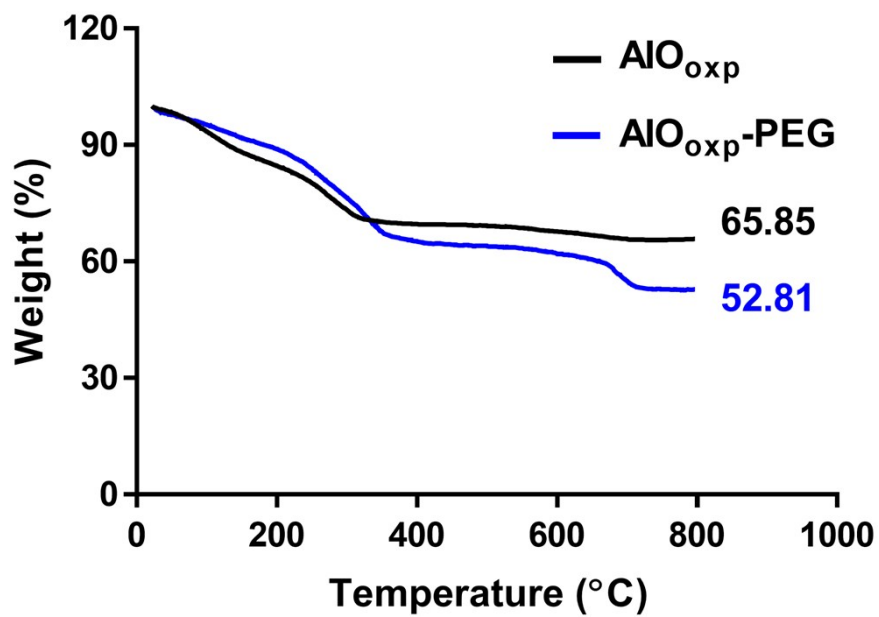


**Figure S6.** Thermogravimetric analysis (TGA) of a dried sample of  $\text{AlO}_{\text{oxp}}$  NPs with or without PEG modifications in the temperature range from room temperature to 800  $^{\circ}\text{C}$  at a heating rate of 10  $^{\circ}\text{C}/\text{min}$  in nitrogen.

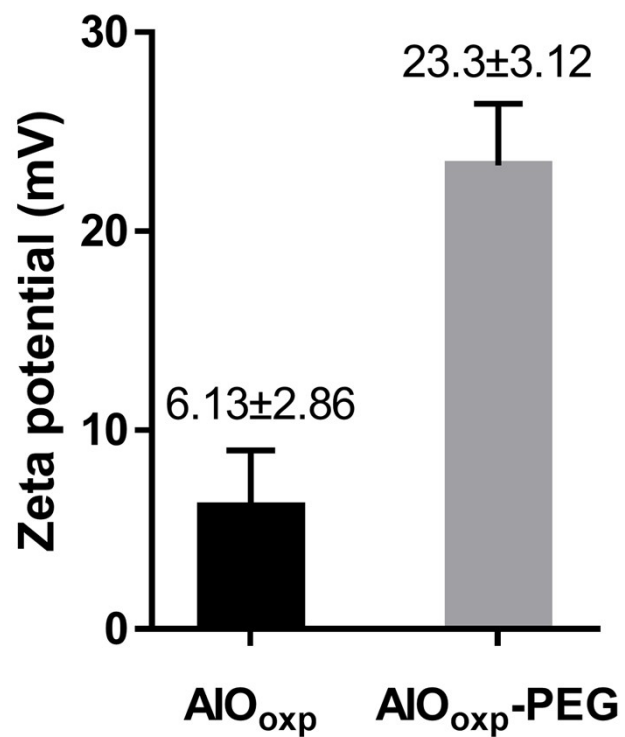


**Figure S7.** Zeta potentials of AIO<sub>oxp</sub> NPs with or without PEG modifications detected by dynamic light scattering.

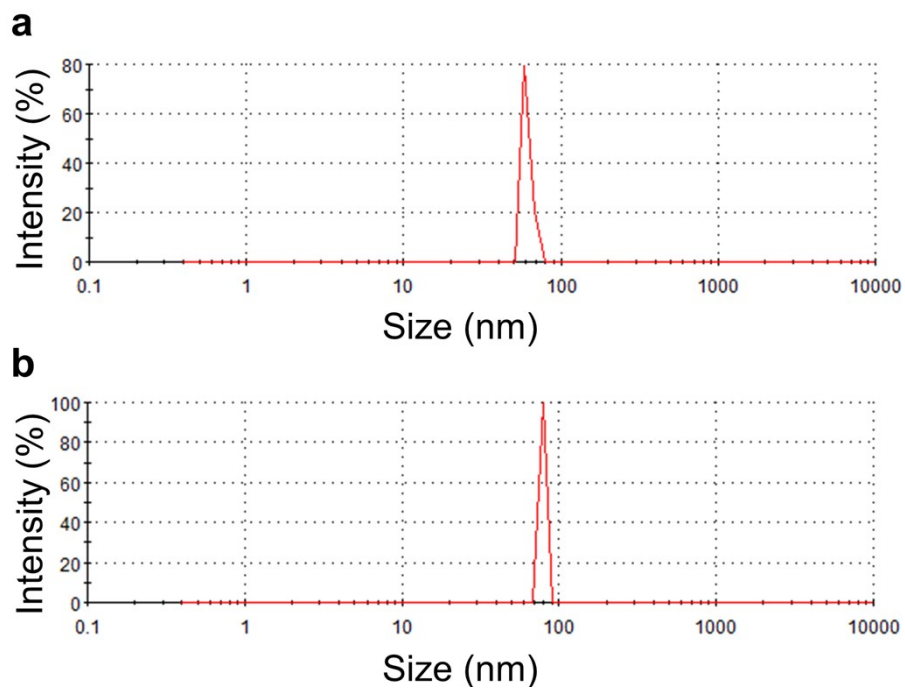


**Figure S8.** The hydrodynamic sizes of AIO NPs (a) and AIO<sub>oxp</sub> NPs (b) in PBS detected by dynamic light scattering.

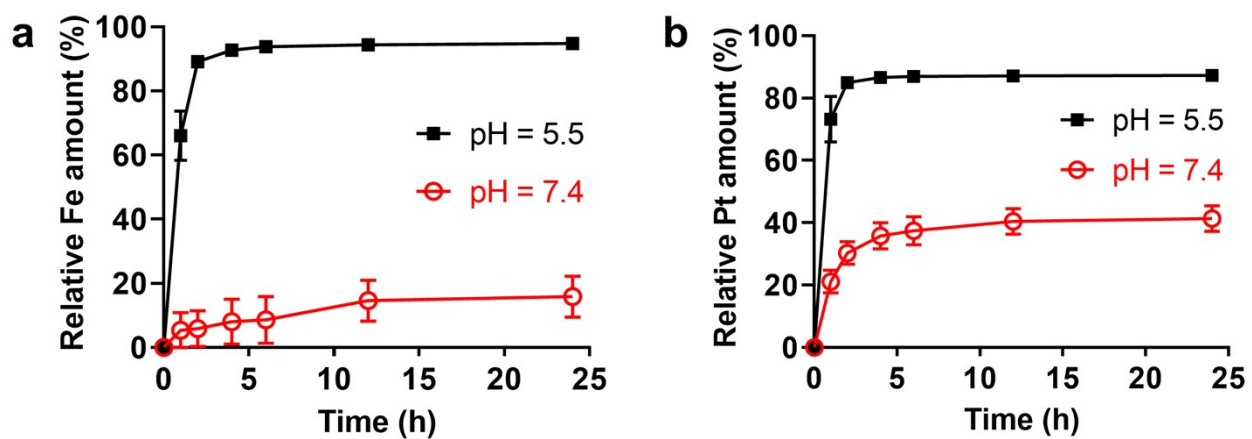


**Figure S9.** The (a) Fe and (b) Pt release profiles from AIO<sub>oxp</sub> in PBS solution under different pH (5.5 and 7.4).

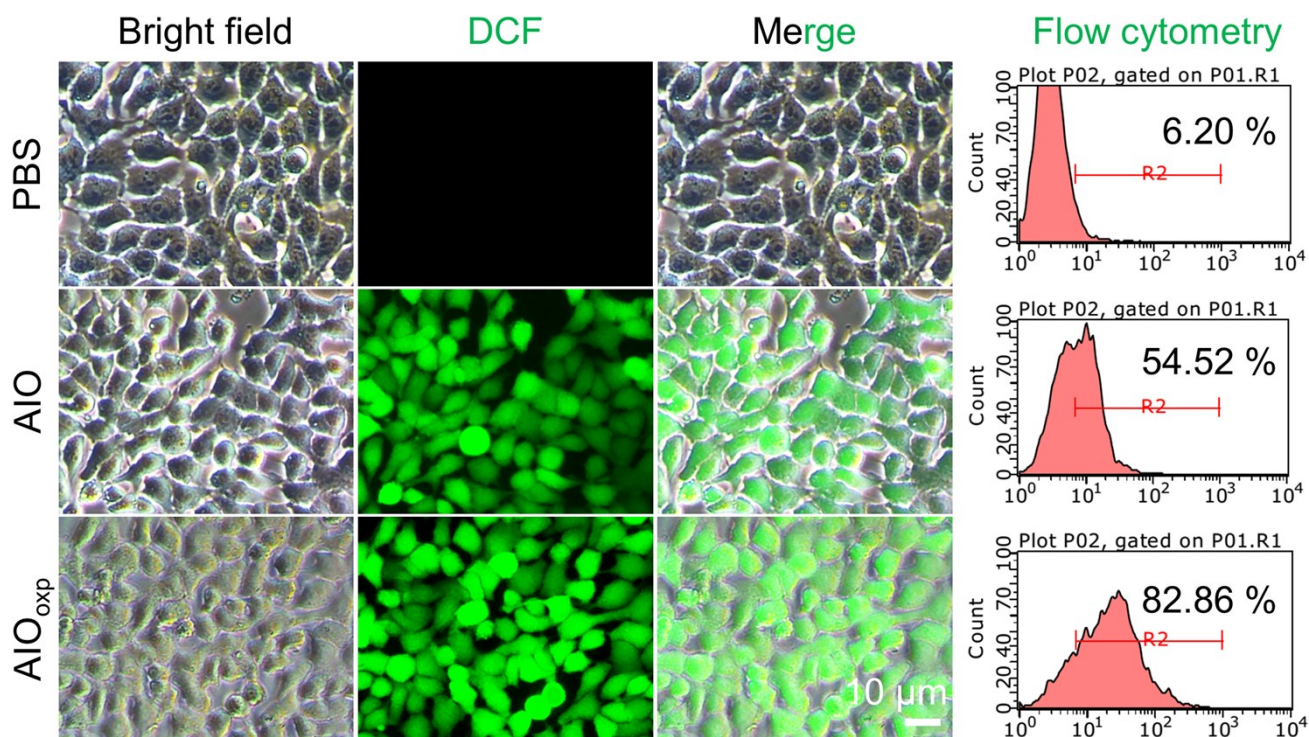


**Figure S10.** Intracellular ROS detections of 4T1 cells treated with PBS, AIO NPs or AIO<sub>oxp</sub> NPs stained with 2',7'-dichlorodihydrofluorescein (DCFH-DA) which can be rapidly oxidized to 2',7'-dichlorofluorescein (DCF) with green fluorescence by ROS. A quantitative analysis by flow cytometry about DCF with different treatments.

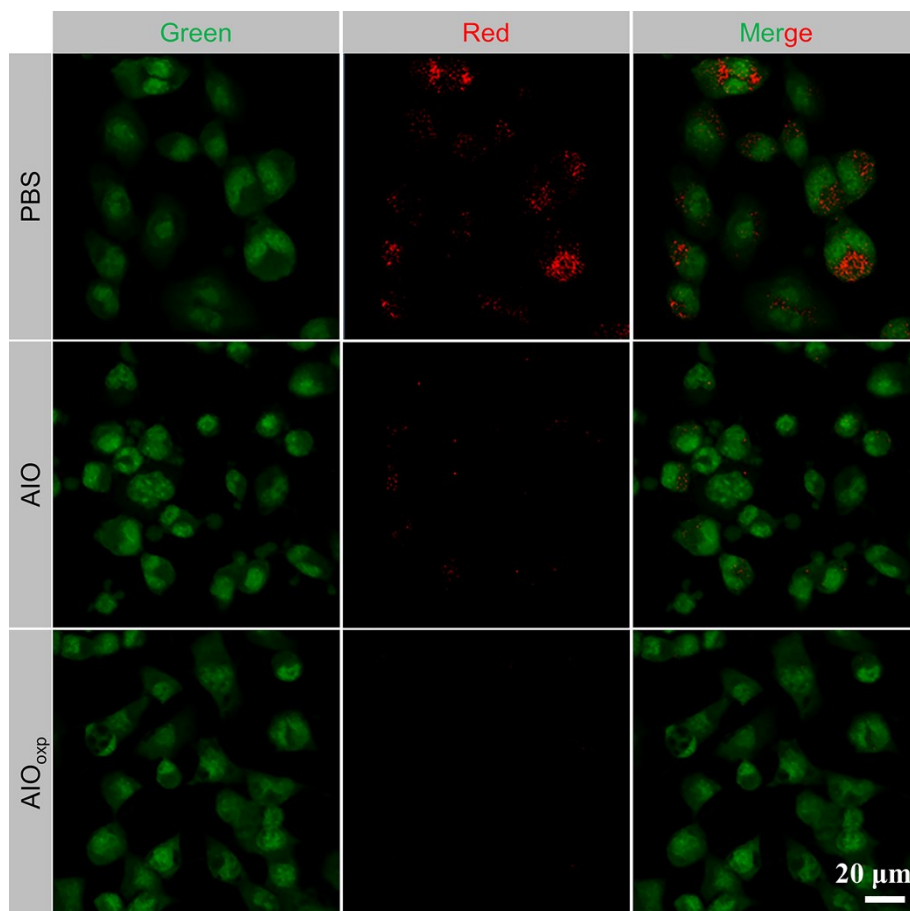


**Figure S11.** AO staining of 4T1 cells treated with PBS, AIO NPs or AIO<sub>oxp</sub> NPs. The reduced red dots suggest the loss of membrane integrity of endo/lysosomes.

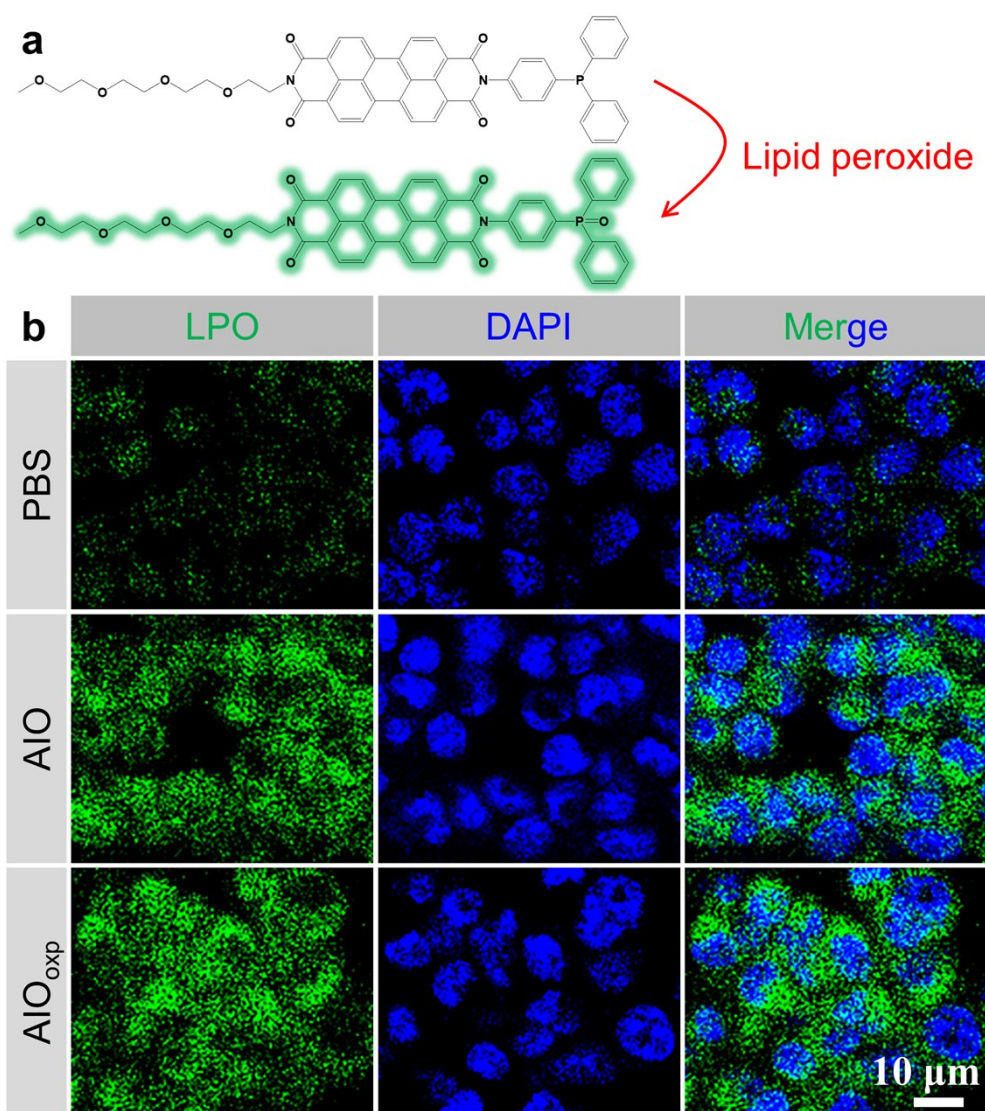


**Figure S12.** (a) Schematic illustration of the intracellular LPO detection using Liperfluo probes. (b) Intracellular LPO detections of 4T1 cells treated with PBS, AIO NPs or AIO<sub>oxp</sub> NPs stained with LPO probe Liperfluo.

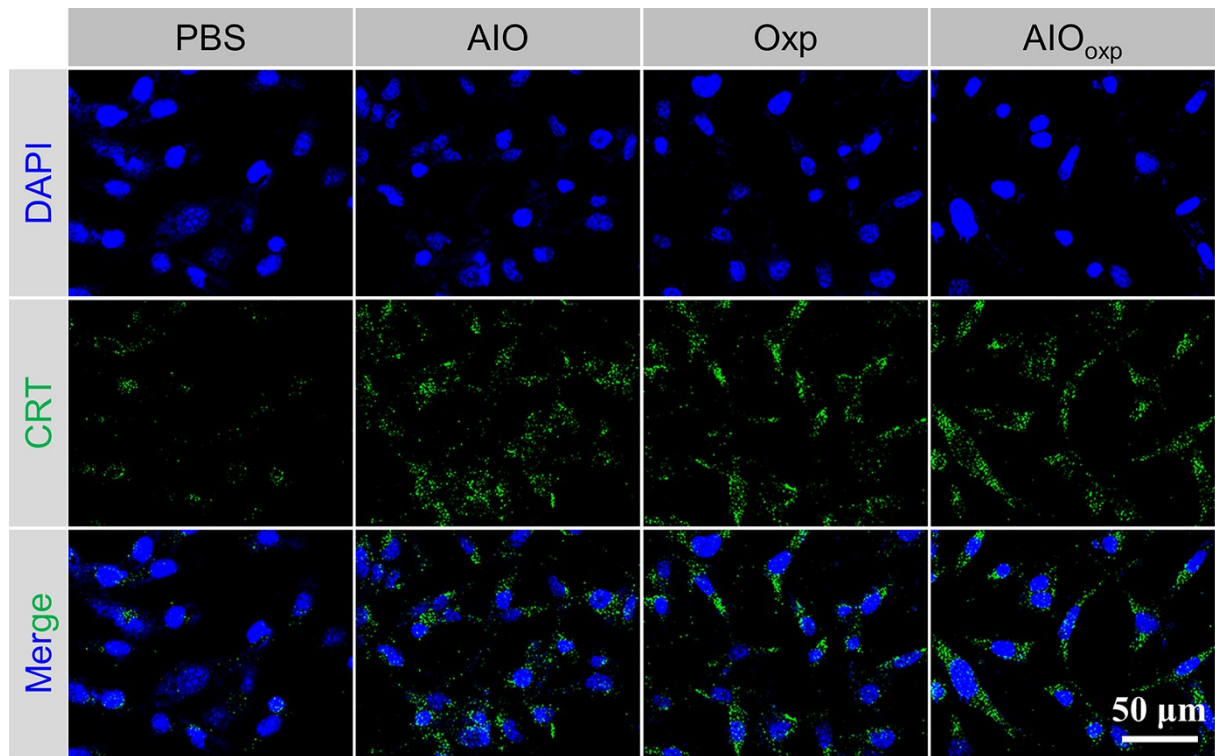


**Figure S13.** Calreticulin (CRT) exposure of 4T1 cells treated with PBS, AIO NPs, Oxp or AIO<sub>oxp</sub> NPs.

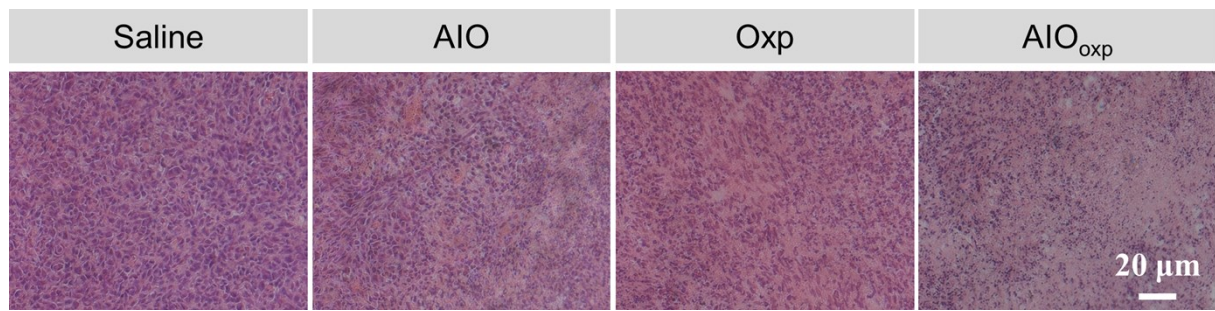


**Figure S14.** H&E staining images for tumor after various treatments (Saline, AIO NPs, Oxp or AIO<sub>oxp</sub> NPs).

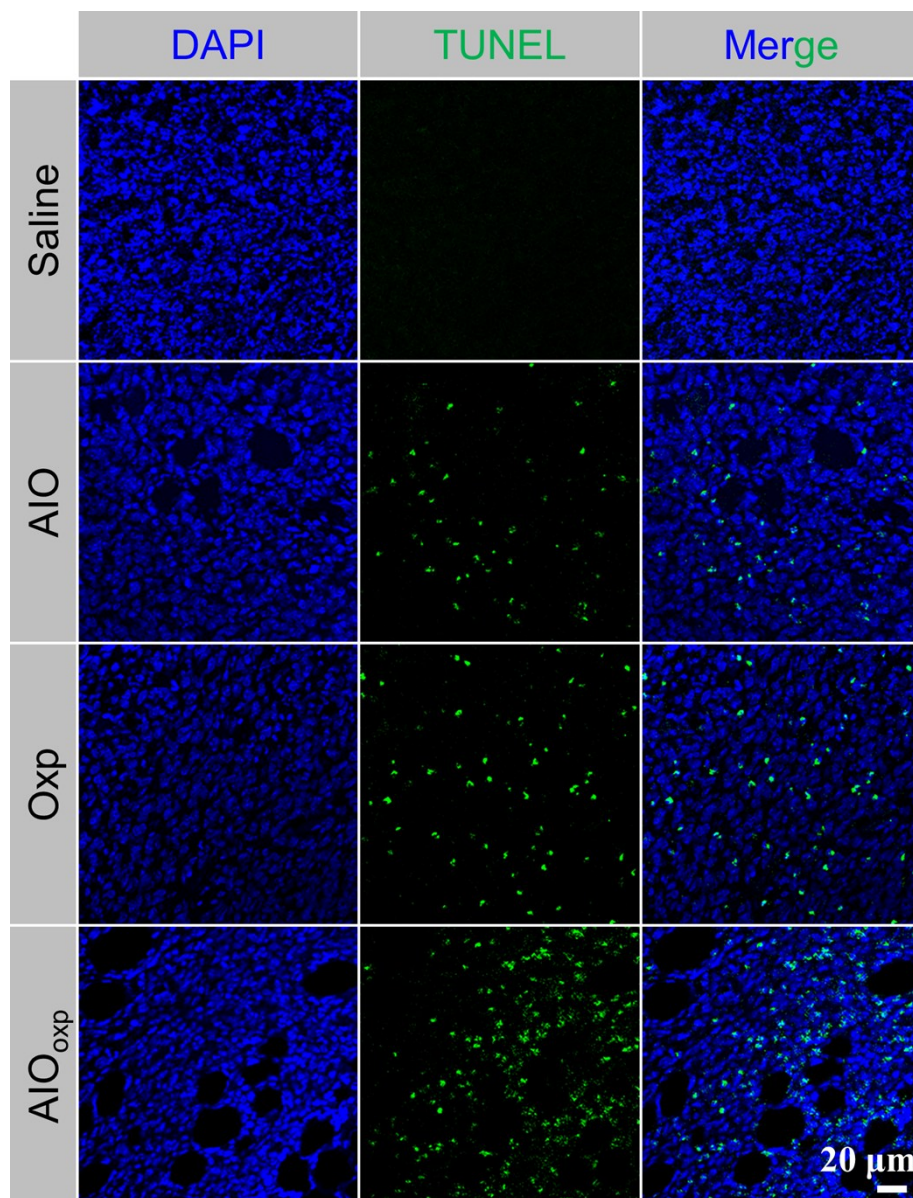


**Figure S15.** TUNEL staining images for tumor after various treatments (Saline, AIO NPs, Oxp or AIO<sub>oxp</sub> NPs).

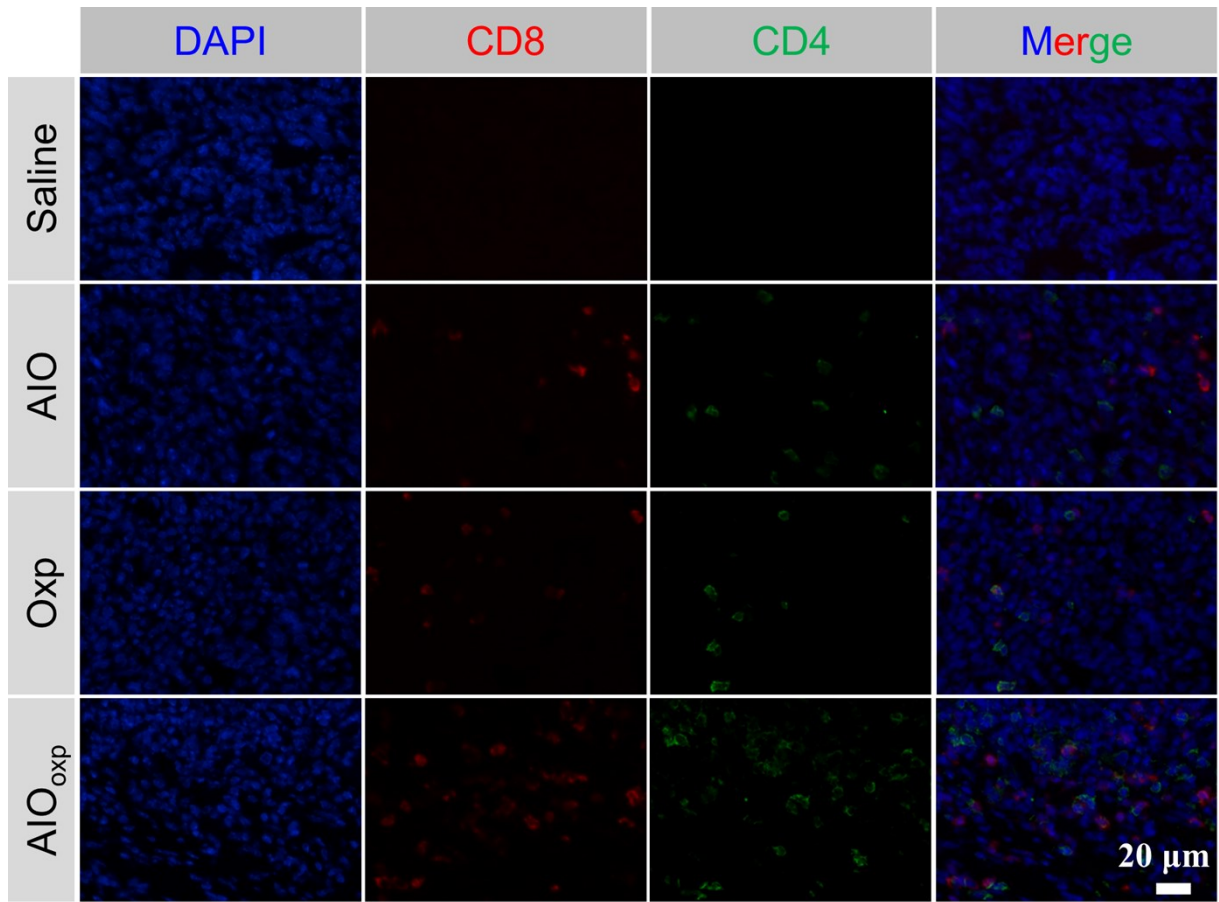


**Figure S16.** CD8 (red) and CD4 (green) stainings of tumors with different treatments (Saline, AIO NPs, Oxp or AIO<sub>oxp</sub> NPs).

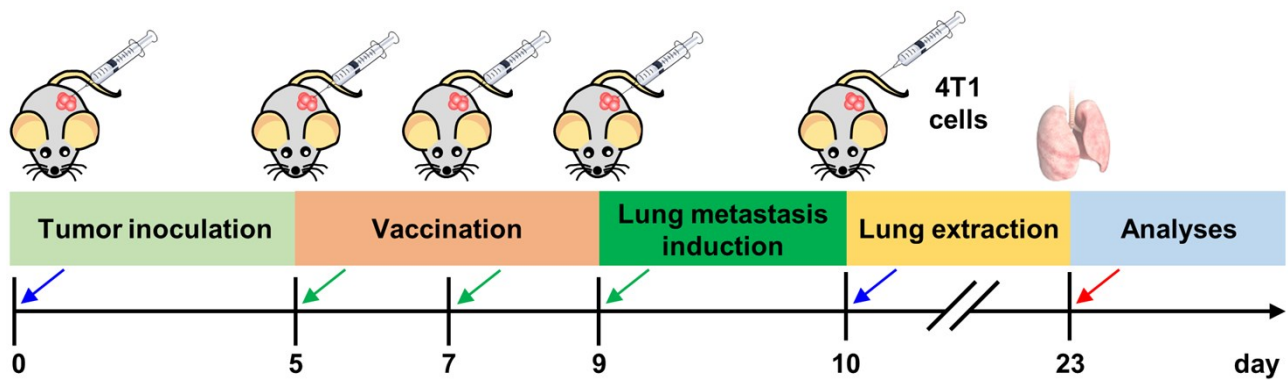


**Figure S17.** Therapeutic schedule for AIO<sub>oxp</sub> NPs-induced inhibition of tumor metastasis.

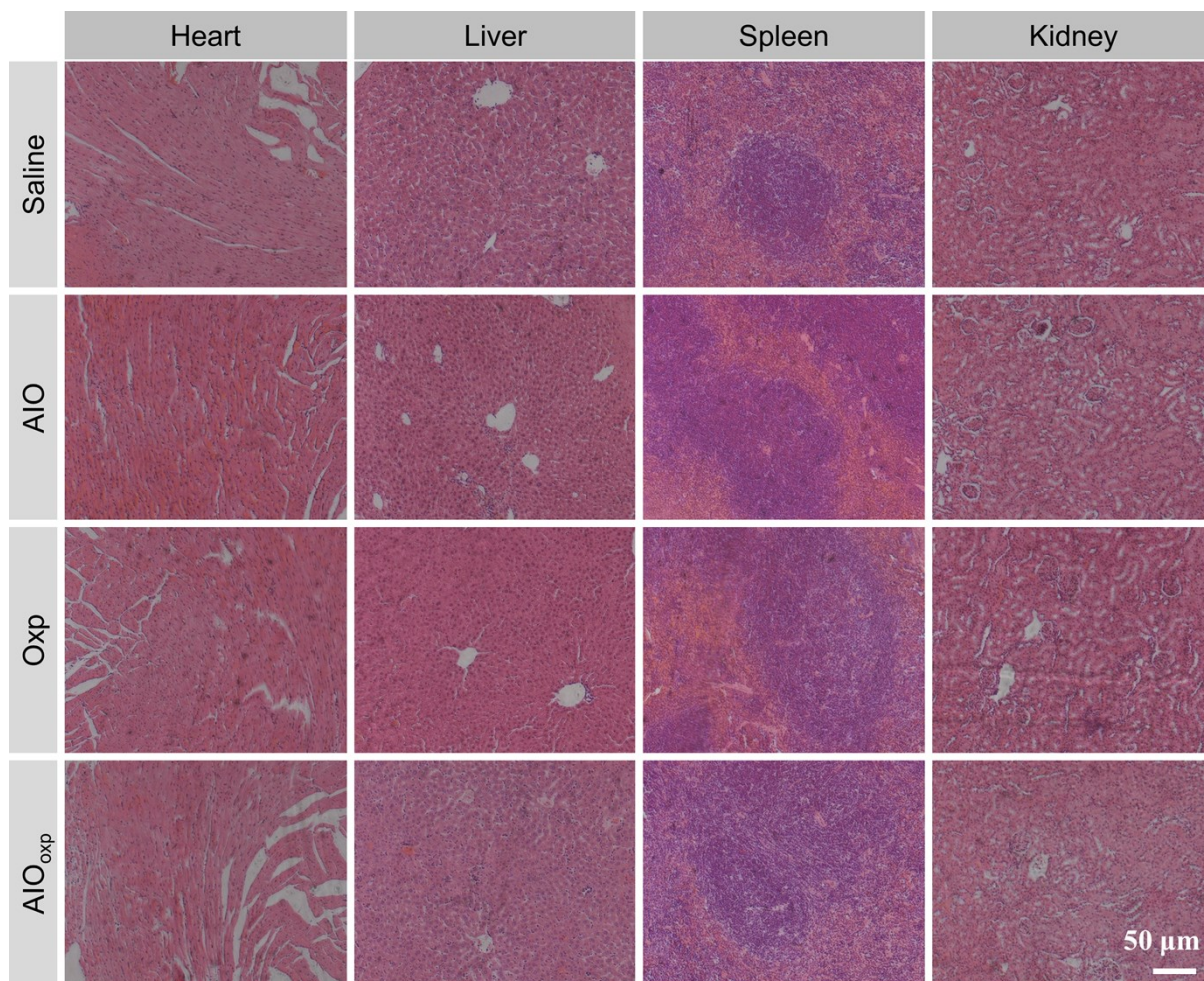


**Figure S18.** H&E-stained images of major organs of BALB/c mice after different treatments (Saline, AIO NPs, Oxp or AIO<sub>oxp</sub> NPs) in antimetastatic studies, including heart, liver, spleen and kidney.

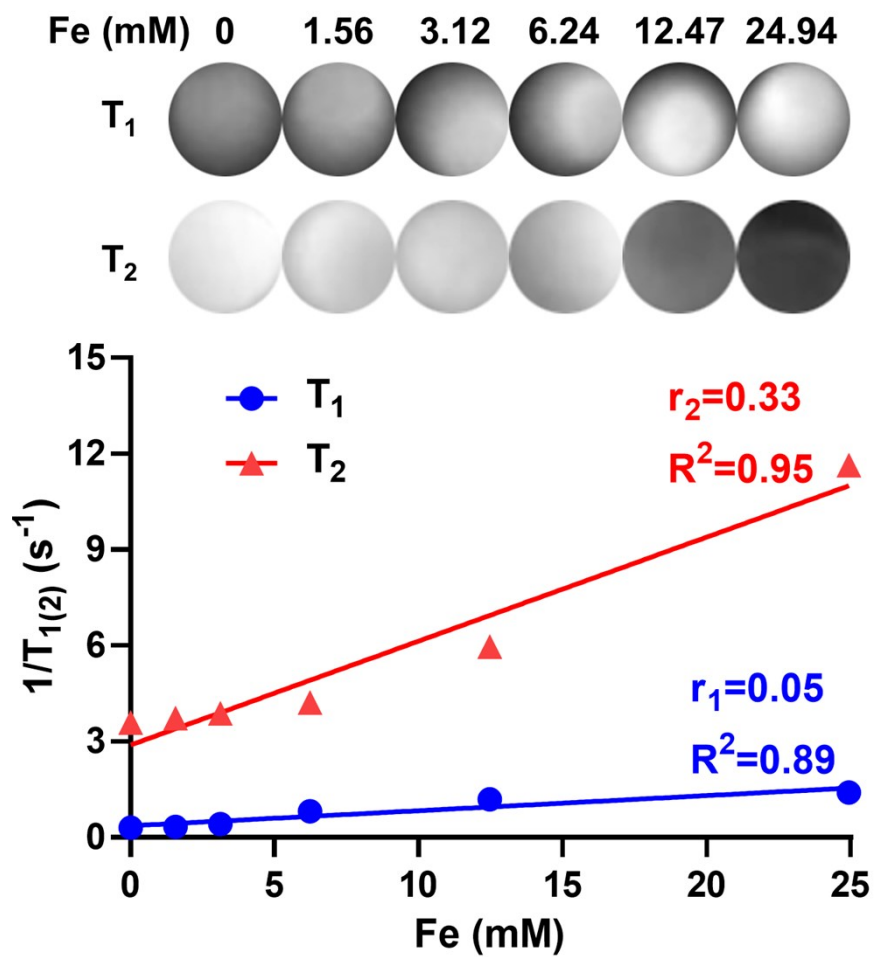


**Figure S19.** In vitro  $T_1/T_2$ -weighted MRI of AIO NPs aqueous solution at different Fe concentrations and  $T_1/T_2$  relaxation time ( $r_1=0.05 \text{ mM}^{-1}\text{s}^{-1}$ ;  $r_2=0.33 \text{ mM}^{-1}\text{s}^{-1}$ ).

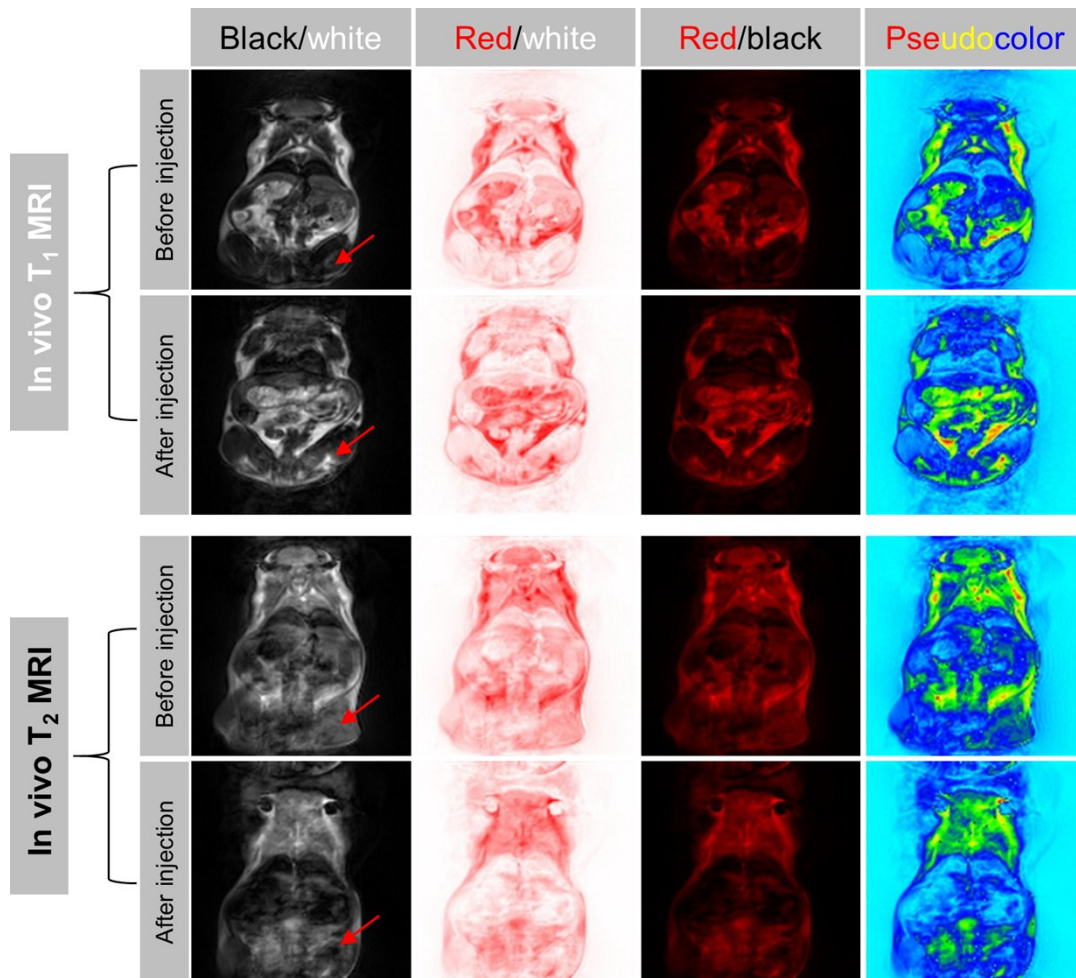


**Figure S20.** In vivo T<sub>1</sub>/T<sub>2</sub>-weighted MRI before and after injection of AIO NPs.